Influence of electric field on local phase transformations in relaxor ferroelectrics PbSc 0.5 Ta 0.5 O 3 and Pb 0.78 Ba 0.22 Sc 0.5 Ta 0.5 O 3

B. J. Maier, T. Steilmann, M. Gospodinov, U. Bismayer, and B. Mihailova

Citation: Journal of Applied Physics **112**, 124111 (2012); doi: 10.1063/1.4770479
View online: http://dx.doi.org/10.1063/1.4770479
View Table of Contents: http://scitation.aip.org/content/aip/journal/jap/112/12?ver=pdfcov
Published by the AIP Publishing

Influence of electric field on local phase transformations in relaxor ferroelectrics $PbSc_{0.5}Ta_{0.5}O_3$ and $Pb_{0.78}Ba_{0.22}Sc_{0.5}Ta_{0.5}O_3$

B. J. Maier,[1,2,a)] T. Steilmann,[1] M. Gospodinov,[3] U. Bismayer,[1] and B. Mihailova[1,b)]
[1]*Department Geowissenschaften, Universität Hamburg, 20146 Hamburg, Germany*
[2]*Department für Geo- und Umweltwissenschaften, Ludwig-Maximilians-Universität München, 80333 München, Germany*
[3]*Institute of Solid State Physics, Bulgarian Academy of Sciences, Blvd. Tzarigradsko Chausse 72, 1784 Sofia, Bulgaria*

(Received 4 September 2012; accepted 27 November 2012; published online 21 December 2012)

In situ temperature-dependent Raman-scattering experiments under an external dc electric field E have been performed on $PbSc_{0.5}Ta_{0.5}O_3$ (PST) and $Pb_{0.78}Ba_{0.22}Sc_{0.5}Ta_{0.5}O_3$ (PST-Ba) in order to give further insights into the atomistic mechanism of polar coupling in perovskite-type (ABO_3) relaxor ferroelectrics near the intermediate characteristic temperature $T^\star$. The polarized Raman spectra collected under an electric field E applied along the cubic [100], [110], or [111] crystallographic direction were analyzed in terms of hard-mode spectroscopy. The $T^\star(E)$ dependence was derived from the behavior of the phonon mode near 230 cm^{-1} localized in off-centered B-site cations. In the case of stoichiometric PST, the increase of $T^\star$ with E is much stronger when the field is applied along [111] than when E is along [100] or [110]. This indicates that the actual polar B-cation shifts are along the cubic body diagonals, implying a rhombohedral structure of the polar nanoregions. The $T^\star(E)$-dependence reveals that the local structural distortions associated with locally coupled polar displacements of B-site cations reach saturation near 0.5 kV/cm. When Pb^{2+} is partially replaced by Ba^{2+}, the strong increase of $T^\star$ with E occurs if the electric field is applied along the [110] direction. This indicates that the substitution disorder on the A-site lowers the symmetry of the polar nanoregions to orthorhombic or monoclinic. The $T^\star(E)$ dependence determined from the B-cation localized mode shows saturation near 2.0 kV/cm, indicating that the zero-field structural state of PST-Ba exhibits less coupled polar shifts of B-site cations as compared to that of PST. According to the E-dependence of the Raman scattering near 55 cm^{-1}, for both compounds the overall response of the Pb system to the external electric field in the vicinity of $T^\star(E)$ resembles antiferroelectric behavior, which along with the fact that the coupling between the B-site cations is ferroelectric, suggests that the polar nanoregions in Pb-based relaxors are *ferrielectric* in nature. © *2012 American Institute of Physics*. [http://dx.doi.org/10.1063/1.4770479]

I. INTRODUCTION

Lead-based relaxor ferroelectrics with the perovskite-type structure (ABO_3) are important materials for technological applications due to their outstanding dielectric, electro-optic, and electromechanical properties which are related to the complex nanoscale structure.[1] Relaxors exhibit a broad and frequency-dependent maximum of the dielectric permittivity as a function of temperature due to the existence of polar nanoregions (PNRs), which exhibit life times on the microsecond scale near the temperature of the dielectric permittivity maximum T_m.[2] Four important temperatures are associated with the temperature evolution of PNRs: T_B, $T^\star$, T_m, and T_f for canonical relaxors or T_C for relaxors developing ferroelectric long-range ordering at low temperatures. Polar nanoclusters nucleate at the Burns temperature T_B at which the refractive index deviates from the linear trend typical of paraelectrics.[3] These polar nanoclusters couple at another for relaxors characteristic temperature, $T^\star$,[4–6] at which larger PNRs with slower dynamics are formed.[7] Below T_m the PNRs either become static at the so-called freezing temperature T_f resulting in a thermodynamically non-ergodic state or evolve into long-range ordered ferroelectric domains at the Curie temperature T_C.[1]

Recently, two model relaxor ferroelectrics $PbSc_{0.5}Ta_{0.5}O_3$ (PST), which on cooling undergoes a phase transition to a long-range-ordered ferroelectric state, and $Pb_{0.78}Ba_{0.22}Sc_{0.5}Ta_{0.5}O_3$ (PST-Ba), which is a canonical relaxor with the average structure remaining cubic below T_m, have been studied by acoustic emission under an external electric field.[8] A shift of T_C (for PST-Ba field-induced above 0.5 kV/cm) and $T^\star$ to higher temperatures with increasing electric field E has been observed for both compounds. It was found that the slope of $T^\star(E)$ is steeper than the slope of $T_C(E)$ for both compounds due to enhanced local electric fields inside PNRs in the vicinity of $T^\star$. In addition, an acoustic emission signal exhibiting a V-type E-dependence was detected at T_n lying between T_m and $T^\star$. The temperature T_n has been attributed to the formation of antiferroelelctric order, coexisting on the mesoscopic scale with the polar order.[8]

Acoustic emission is however a method which detects the elastic strain developed on the boundary between regions with different atomic structure, i.e., it represents the macroscopic

a)Electronic mail: bernd.maier@lmu.de.
b)Electronic mail: boriana.mihailova@uni-hamburg.de.

response of the whole system (paraelectric matrix—polar nanoregions) near $T^{\star}$. On the other hand, Raman spectroscopy is a method that can directly probe the development of ferroic atomic arrangements by analyzing the temperature dependence of the phonon anomalies, giving rise to "forbidden" Raman peaks. Furthermore, the application of an external electric field effectively reduces the symmetry of the system and thus changes the selection rules in a way depending on the direction of the applied field.[9] For the relaxor state, which comprises polar and cubic matter, the external electric field should have the strongest effect on the anomalous Raman peaks arising from PNRs when the direction of E lowers the cubic symmetry in the same manner as the group-subgroup relation between the paraelectric phase and the atomic structure of PNRs. Hence to further elucidate the atomic arrangements of PNRs and to study the ferroic coupling in the ergodic relaxor state above T_m in terms of off-centered cations involved, we applied *in situ* polarized Raman spectroscopy at different temperatures on PST and PST-Ba single crystals subjected to an external electric field along the cubic [100], [110], and [111] directions (see Fig. 1).

II. EXPERIMENTAL DETAILS

Cube-shaped PST and PST-Ba single crystals of optical and chemical homogeneity were synthesized by the high-temperature solution crystal growth method. The chemical composition was verified by electron microprobe analysis (Cameca microbeam SX100 SEM system), by averaging over 100 spatial points on each sample. Both samples possess a very low degree of chemical B-site order, as determined by x-ray diffraction.[10] Plane-parallel plates approximately 1 mm thick were cut parallel to the cubic (100), (110), and (111) planes. Then, 1-mm thick rods parallel to the cubic [100] direction for the (100) plate and parallel to the cubic [110] direction for the (110) and (111) plates were cut out. Contact wires have been glued to the faces perpendicular to the cubic [100], [110], and [111] directions (see Fig. 1) using PELCO® *High Performance Silver Paste*. Prior to the Raman experiments at different temperatures, the samples with the attached electrical contacts were annealed at 93 °C for 2 h in order to cure the silver paste.

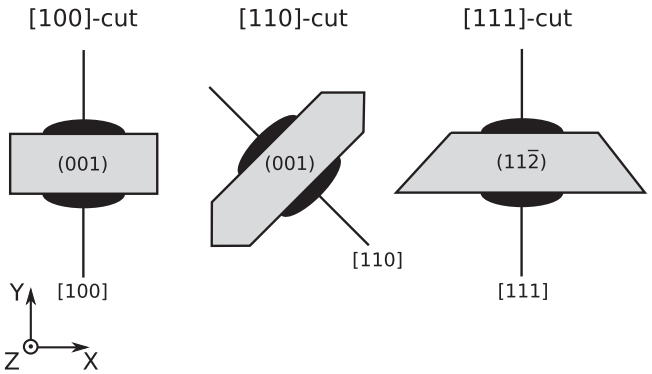

FIG. 1. Sketch of the sample orientation with respect to the laboratory coordinate system (bottom left); the designation of the cuts is according to the cubic crystallographic directions along which the electric field is applied. For all samples, polarized spectra were collected in $\bar{Z}(XX)Z$ and $\bar{Z}(XY)Z$ scattering geometries, where X, Y, and Z are laboratory coordinate axes. The cubic crystallographic planes perpendicular to the direction of the laser beam were (001) for [100]- and [110]-cuts and $(11\bar{2})$ for [111]-cut. The polarization of the incident light was along the cubic [100] direction for [100]- and [110]-cuts and along [110] for [111]-cut.

Raman spectra were collected using a Horiba Jobin-Yvon T64000 triple-grating spectrometer equipped with an Olympus BH41 microscope and a $50\times$ long-working distance objective. The measurements were conducted in backscattering geometry using the 514.5-nm line of an Ar^{+} laser, a spectral resolution of 2 cm^{-1}, and a power density on the sample surface of 2.8 kW/mm^2. The *in situ* temperature-dependent experiments were conducted in a LINKAM heating-cooling stage ensuring a temperature stability of ± 0.1 K. Polarized spectra were collected upon cooling from a maximum temperature of 550–850 K down to a minimum temperature of 80–125 K with temperature steps between 5 and 25 K in $\bar{Z}(XX)Z$ and $\bar{Z}(XY)Z$ scattering geometries (Porto's notation), where X, Y, and Z are parallel to the cubic [100], [010], and [001] crystallographic directions, respectively, for the (100) and (110) cut. In the case of the (111) cut, X, Y, and Z are parallel to the cubic [110], [111], and $[11\bar{2}]$ directions, respectively.

The as-measured spectra were reduced by $n(\omega,T)+1$, where $n(\omega,T)=1/(e^{\hbar\omega/kT}-1)$ is the Bose-Einstein phonon distribution in order to eliminate the effect of temperature on the peak intensities. Subsequently, the spectra measured in $Z(XX)\bar{Z}$ and $Z(XY)\bar{Z}$ geometries at each temperature were normalized to the sum of their integral intensity. The normalized spectra were fitted with Lorentzian functions to determine the peak positions, full widths at half maximum (FWHMs) and integrated intensities, using the software FITYK.[11] No constraints were imposed on the peak parameters during the fitting procedure. Examples of the performed multiple peak fitting procedure are shown in Fig. 2. Detailed symmetry analysis of the observed peaks and their assignment to definite atomic vibrations are given in Refs. 12 and 13, revealing that the Raman spectra should be interpreted in terms of a double perovskite structure (aristotype $Fm\bar{3}m$).

III. RESULTS AND DISCUSSION

Hard-mode analysis of polarized Raman spectra is a great tool to study phase transformations occurring in relaxors and has been successfully applied in our previous studies on PST and PST-Ba under zero-field cooling.[7,14] It has been shown that $T^{\star}$ can be determined from the abrupt sharpening of the Raman peak near 240 cm^{-1} originating from off-centered B-site cations (see Fig. 3(b)), accompanied by a change in the slope of the wavenumber $\omega(T)$ of the same mode (see Fig. 3(a)), as $\omega(T)$ becomes nearly constant between $T^{\star}$ and T_C.[7] The temperature behavior of the position and FWHM of the 240-cm^{-1} peak represents the saturation of the off-centered displacements and the strong increase in the coherent length of coupled polar shifts of B-site cations.

In the ergodic relaxor state above T_m the Raman scattering near 55 cm^{-1} in the cross polarized $Z(XY)\bar{Z}$ spectra is related mainly to the symmetry-allowed cubic F_{2g} mode (present only in a double-perovskite structure), while the scattering near 55 cm^{-1} in the parallel polarized $Z(XX)\bar{Z}$ spectra originates from phonon anomalies due to the

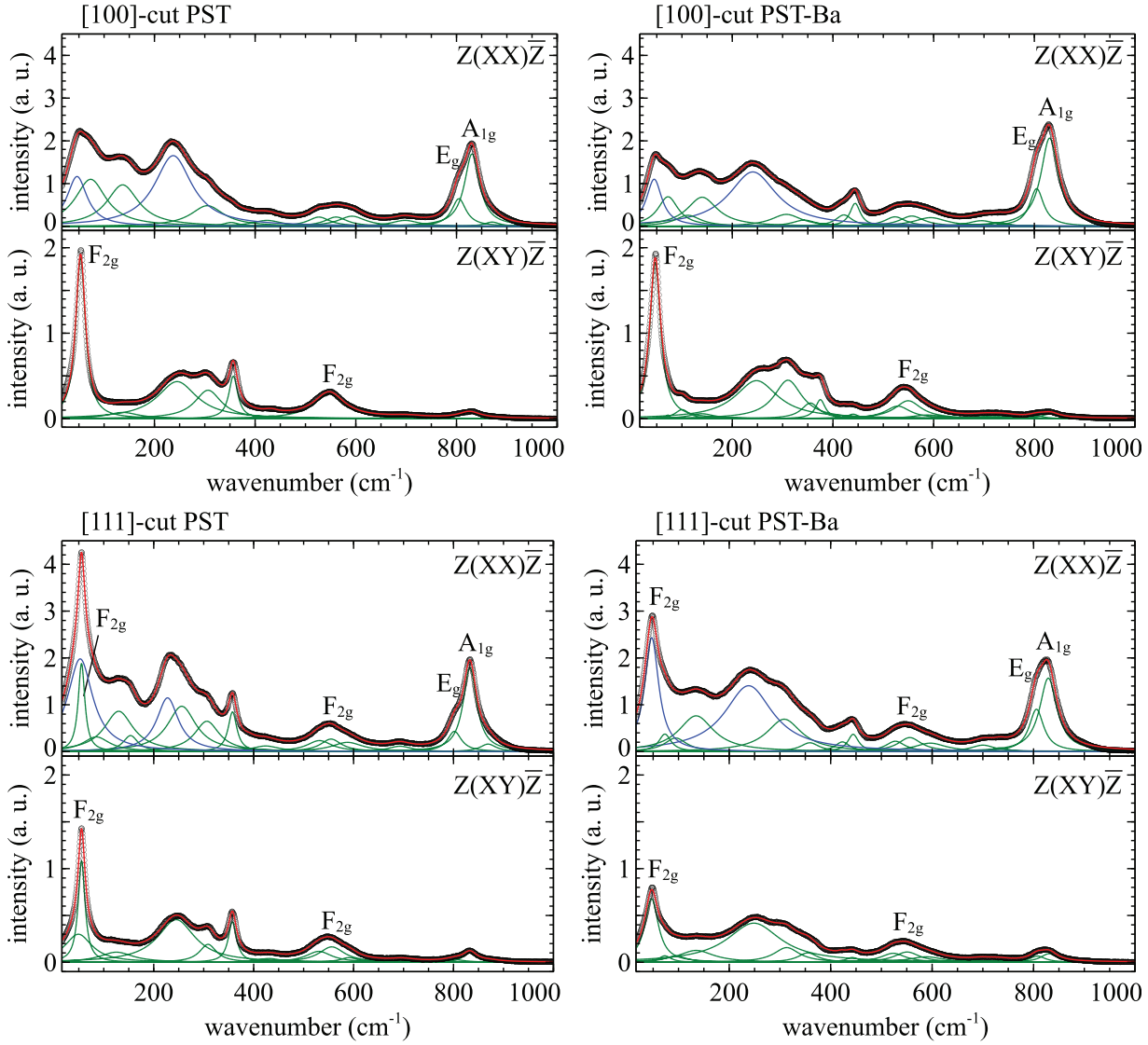

FIG. 2. Multipeak fit of zero-field $Z(XX)\bar{Z}$ and $Z(XY)\bar{Z}$ Raman spectra for [100]- and [111]-cuts of PST and PST-Ba at 295 K. The zero-field spectra for the [110]-cuts are the same as for the [100]-cuts. The experimental spectra are given by open circles. The green dashed lines represent the Lorentzian components of the spectral fit (red line), whereas the anomalous signals of the Pb-localized mode near 55 cm^{-1} and the B-localized mode near 240 cm^{-1} further used to build E-dependences are given by blue solid lines. It should be noted that for [111]-cut PST-Ba the Lorentzian component near 55 cm^{-1} represents a superposition of the signals arising from the cubic F_{2g} mode and the anomalous Pb-localized mode, which could not be discriminated in the fitting procedure, by contrast to the case of PST. The Raman peaks to which the cubic phonon modes of $Fm\bar{3}m$ space group contribute are marked by the corresponding irreducible representations.

presence of off-centered Pb cations in the double-perovskite structure.[12,13] In the case of a para-to-ferroelectric phase transition, the latter vibrations evolve in phonon modes of the rhombohedral ferroelectric phase.[7] The temperature dependence of the wavenumber ω of this anomalous Pb-localized phonon mode (see Fig. 4(a)) reveals that the temperature decrease induces stepwise transformations in the system of off-center displaced Pb^{2+} cations. The stepwise softening of $\omega(T)$ near $T^{\star}$ reveals that the system of off-centered Pb^{2+} cations enters a metastable state, whereas the hardening near T_C reflects the growth of polar nanoregions into long-range ferroelectric domains, i.e., stabilization of the ferroelectric order. It should be emphasized that canonical relaxors like PST-Ba, which do not exhibit a phase transition below T_m, show similar temperature behavior of the anomalous Pb-localized mode.[7]

Since the occurrence of a phase transition reflects also on the FWHM of the Raman peak generated by the phonon mode involved in the structural alteration,[15] we focused on the temperature dependence of the FWHM of the Raman scattering near 55 cm^{-1}.[15] Recently, it has been suggested that the off-centered Pb atoms may experience ferroelectric as well as antiferroelectric coupling.[16–18] However, the temperature dependence of the $Z(XX)\bar{Z}$ Raman peak, namely softening below T_B, hardening above T_C, indicates that it is related to off-centered Pb cations inside the polar nanoregions. On the other hand, the doubling of the perovskite structure on the mesoscopic scale should be related not only to the local 1:1 chemical order on the B-site but also to the existing local antiferrodistortive order. Hence, the latter should be present in both polar and non-polar spatial regions and should influence the anomalous as well as the allowed

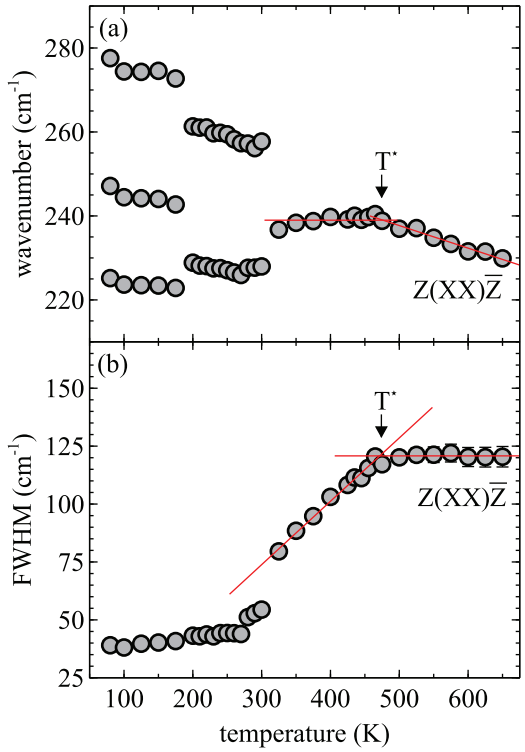

FIG. 3. Temperature dependence of the wavenumber (a) and the FWHM (b) of the Raman peak near 240 cm^{-1} generated from off-centered B-site cations for [111]-cut PST under zero-field cooling. The red lines represent linear fits.

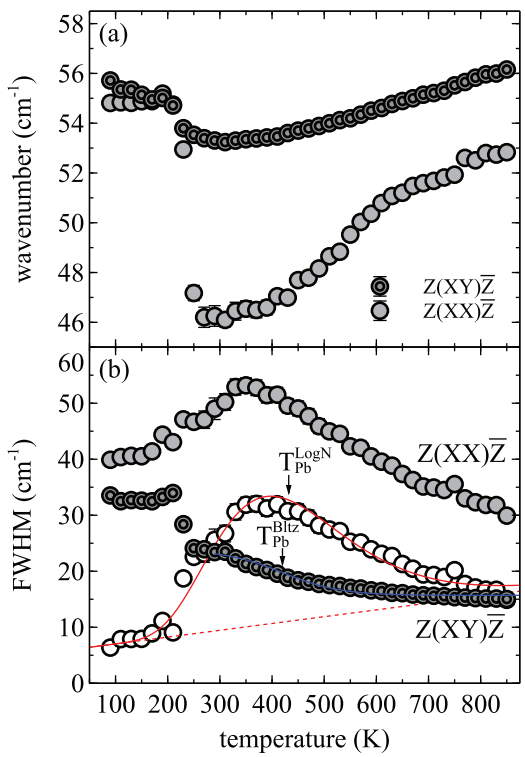

FIG. 4. Temperature dependence of the wavenumber (a) and FWHM (b) of the cubic (dark-gray double circles) and anomalous (gray circles) signal of the Pb-localized mode near 55 cm^{-1} for [100]-cut PST. The blue line represents a Boltzmann fit in the range 290–850 K with an inflection point marked by T_{Pb}^{Bltz}. The open circles represent the difference of the two signals while the red line represents a peak fit using a Log Normal peak profile with a baseline (red dashed line). The mean value of the Log Normal function is marked by T_{Pb}^{LogN}.

Pb-localized phonon modes. Indeed, the FWHM of both $Z(XX)\bar{Z}$ and $Z(XY)\bar{Z}$ Raman peaks near 55 cm^{-1} exhibits non-trivial temperature behavior (see Fig. 4(b)).

The FWHM of the anomalous signal as a function of temperature shows a very broad asymmetric maximum with a baseline which, instead to gradually decrease on cooling,[15] follows the temperature dependence of the Raman scattering arising from the non-polar matrix. Hence, we fitted the difference in FWHM of the anomalous and allowed signal with an asymmetric Log-Normal function to gain an independent estimation of the structural transformations of Pb atoms in the polar nanoregions and further analyzed the electric-field dependence of the mean value T_{Pb}^{LogN} (see Fig. 4(b)).

The increase in the FWHM of the allowed cubic Raman scattering near 55 cm^{-1} with temperature decrease can be attributed to the increased structural disorder in the paraelectric matrix, resulting from the temperature-driven development of interface between polar and non-polar regions as well as possible ferroic Pb shifts in the non-polar fraction. A careful examination of the FWHM of the $Z(XY)\bar{Z}$ signal for PST reveals that it can be fitted using a double Boltzmann function with one component in the range 80–290 K and another in the range 290–850 K (Fig. 4(b)). The low-temperature component

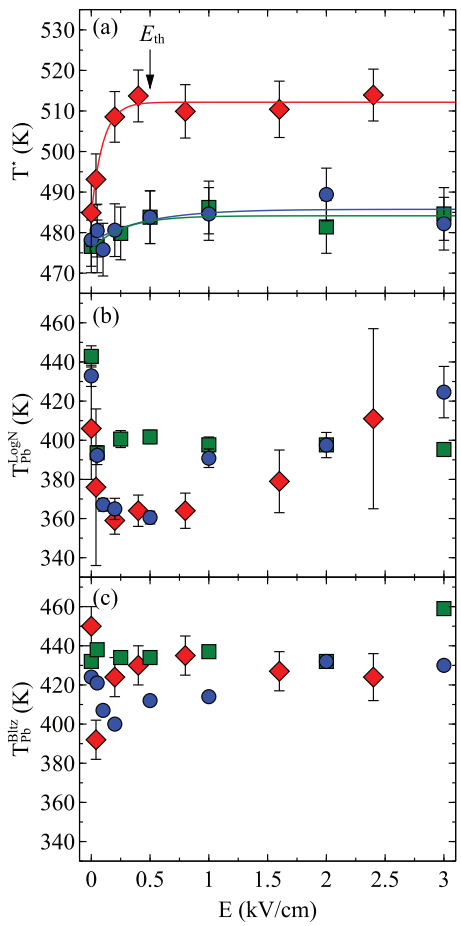

FIG. 5. (a) Electric-field dependence of T^* as deduced from the B-localized mode (see Figs. 3(a) and 3(b)) and of T_{Pb}^{LogN} (b) and T_{Pb}^{Blitz} (c) as deduced by the values of T_{Pb} obtained from the Pb-localized mode (see Fig. 4 for details) for [100]-cut (blue circles), [110]-cut (green squares), and [111]-cut (red diamonds) PST. The lines in (a) represent asymptotic fits ($y = a - bx^c$).

corresponds to the para-to-ferroelectric phase transition and is ascribed to the development of ferroelectric domains, while the high-temperature component should reflect the structural changes of the Pb system in the ergodic state. It should be noted that for PST-Ba a low-temperature kink in the FWHM(T) could hardly be resolved even for high electric fields, which indicates the small fraction of field-induced ferroeletric domains.

Figure 5(a) shows the $T^\star(E)$ dependence determined from the B-site localized mode for PST with the electric field applied along the cubic [100], [110], and [111] directions. A striking result is that the shift of $T^\star$ is small if the electric field is applied along the cubic [100] or [110] directions, whereas there is a strong shift of $T^\star$ to higher temperatures in the case of electric field applied along the cubic [111] direction, i.e., E along the cubic body diagonal facilitates the development of polar order on the mesoscopic scale. This clearly shows that for PST the preferred direction of coupled polar shifts of the B-site cations is along the cubic body diagonal, indicating a rhombohedral configuration of PNRs in PST. This result is in full agreement with the rhombohedral symmetry of PNRs in $Pb(B'_{1/3}B''_{2/3})_{1-x}Ti_xO_3$ deduced from neutron scattering.[19]

The shift of the "microscopic" $T^\star$ to higher temperatures saturates at electric fields above 0.5 kV/cm (Fig. 5(a)), in contrast to the linear trend of $T^\star(E)$ observed for [100]-cut crystal plates by acoustic emission up to $E = 2.5$ kV/cm.[8] It should be emphasized that acoustic emission is a method sensitive to the strain field caused in the cubic matrix by the coupling of the polar nanoclusters at the vicinity of $T^\star$ on a macroscopic scale, whereas Raman scattering probes the actual ferroic distortion in terms of atomic displacements. Hence, the comparative analysis of $T^\star(E)$ derived from the B-cation localized mode (this study) and from acoustic emission[8] indicates that the actual structural distortion that involves coupled off-center shifts of B-site cations saturates above a threshold field $E_{th} \sim 0.5\,\mathrm{kV/cm}$, whereas the size and fraction of polar nanoregions increase linearly with the increase in the electric field.

Figures 5(b) and 5(c) display the E-dependences of T_{Pb}^{LogN} and T_{Pb}^{Bltz} representative for the Pb-cation rearrangements in the PNRs and the non-polar matrix, respectively, when the electric field was applied along different cubic crystallographic directions of PST. For [100]- and [111]-cuts the characteristic temperatures T_{Pb}^{LogN} and T_{Pb}^{Bltz}, describing the transformation of the Pb system in the ergodic state, initially decrease with the increase of E and after reaching a threshold field, they start to increase. This trend resembles the E-dependence of the critical temperature for antiferroelectrics that undergo a field-induced crossover to a ferroelectric state.[20,21] Therefore, the observed $T_{Pb}^{LogN}(E)$ and $T_{Pb}^{Bltz}(E)$ dependences indicate that the Pb cations experience antiferroelectric coupling with a maximum slightly below $T^\star$. It should however be emphasized that this field-induced crossover from antiferroelectric- to ferroelectric-type behavior cannot be explained only within the framework of classical paraelectric-to-antiferroeelctric phase transitions and other mechanisms such as chemically induced random fields should be evoked.[22] For the [110]-cut, $T_{Pb}^{LogN}(E)$ also has a minimum but the increase with E after the threshold field is very weak; for this cut, T_{Pb}^{Bltz} does not show a decrease with E at low field values. Although the E-dependences of T_{Pb}^{LogN} and T_{Pb}^{Bltz} do not indicate any preferred direction of the Pb-cation off-centered displacements, it is apparent that in the ergodic relaxor state the Pb cations exhibit antiferroelectric-type coupling, while the B-site cations exhibit ferroelectric coupling. This observation strongly supports the recently proposed ferrielectric nature of polar nanoregions in relaxors.[18]

Figure 6(a) shows the $T^\star(E)$ dependence determined from the B-cation-localized mode for PST-Ba. In contrast to PST, a strong increase of $T^\star$ to higher temperatures is observed if E is applied along the [110] direction. This indicates that the coupled polar shifts of B-site cations for PST-Ba are along the [110] direction, implying that atomic arrangements in PNRs resemble an orthorhombic or monoclinic structure. The lowering of the symmetry of PNRs in PST-Ba should result from the A-site isovalent substitution of Ba^{2+} for Pb^{2+}, which generates local elastic stresses along the three-fold axes of the adjacent BO_6 octahedra,[23,24] which oppose and thus destabilize the intrinsic (zero-field) polar coupling along the cubic [111] direction. These

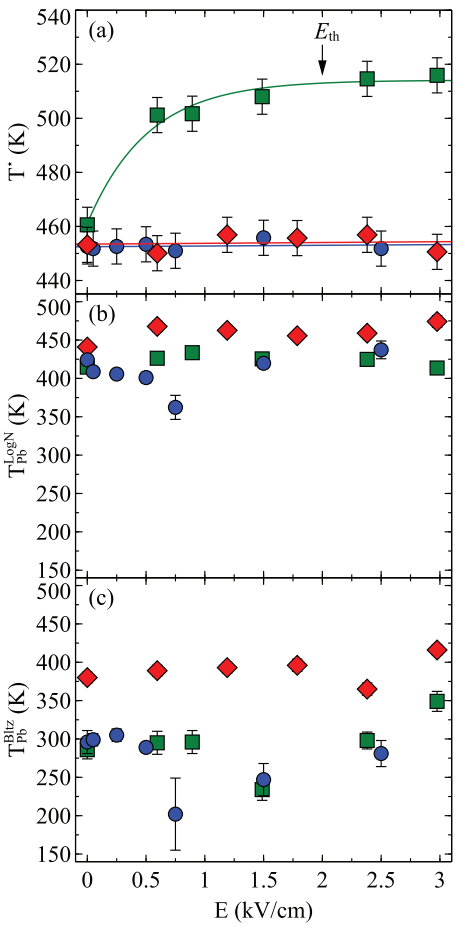

FIG. 6. (a) Electric-field dependence of $T^\star$ as deduced from the B-localized mode (see Figs. 3(a) and 3(b)) and of T_{Pb}^{LogN} (b) and T_{Pb}^{Bltz} (c) as deduced by the values of T_{Pb} obtained from the Pb-localized mode (see Fig. 4 for details) for [100]-cut (blue circles), [110]-cut (green squares), and [111]-cut (red diamonds) PST. The green line in (a) represents an asymptotic fit ($y = a - bx^c$), the other lines are guides for the eye.

doping-induced local elastic stresses have been recently observed by accoustic emission in PST-Ba and PST-La.[25]

Furthermore, the $T^{\star}(E)$ dependence for PST-Ba approaches a constant at higher electric field ($E_{th} \sim 2\,kV/cm$) as compared to PST, i.e., the field-induced B-site cation displacements are saturated at higher E. This indicates that the intrinsic zero-field B-cation coupled polar shifts in PST-Ba are smaller than those in stoichiometric PST.

Similarly to PST, the E-dependences of T_{Pb}^{LogN} and T_{Pb}^{Bltz} of PST-Ba (Figs. 6(b) and 6(c)) reveal antiferroelectric coupling within the Pb-system. By contrast to PST, the V-shaped trends for PST-Ba are better pronounced for $T_{Pb}^{Bltz}(E)$ than for $T_{Pb}^{LogN}(E)$. This might be due to the less fraction and smaller size of PNRs in PST-Ba. The threshold field for PST-Ba determined from the behaviour of the B-cation localized mode (see Fig. 6, upper plot) is higher than that of pure PST (Fig. 5), which is in accordance with the results from acoustic emission.[8] Overall, the threshold field for PST-Ba obtained from the characteristic temperatures of the Pb system is also higher than that for PST. The comparison between $T_{Pb}^{Bltz}(E)$ measured for different PST-Ba cuts indicates that the threshold field is smaller for the [100]-cut and highest for the [111]-cut. Most probably, this is also related to the Ba-induced strong elastic fields along $\langle 111 \rangle$, which oppose to the external electric field to switch the mesoscopic antiferroelectric order to a ferroelectric order.

IV. CONCLUSIONS

The analysis of the *in situ* Raman data collected from PST and PST-Ba at different temperatures under an external field applied along the cubic [100], [110], and [111] directions shows that in the ergodic state the B-site cations couple ferroelectrically, while the A-positioned Pb cations couple antiferrolectrically. Hence, the resultant polarization of PNRs at zero field should be ferrielectric in nature.

Near $T^{\star}$ the preferred direction of coupled polar displacements of B-site cations is along the cubic body diagonal for PST, whereas for A-site Ba-doped PST it is along the cubic face diagonal. This indicates that the symmetry of PNRs in pure PST is rhombohedral and it lowers to orthorhombic/monoclinic upon A-site homovalent doping with Ba. In the case of PST a saturation of the coupled polar displacements of B-site cations was reached at 0.5 kV/cm, in contrast to PST-Ba which reaches saturation near 2 kV/cm. The larger E value of saturation for PST-Ba indicates that the partial substitution of Ba for Pb on the A-site suppresses the initial (intrinsic) zero-field polar coupling near $T^{\star}$.

ACKNOWLEDGMENTS

Financial support by the Deutsche Forschungsgemeinschaft (MI 1127/5-1) is gratefully acknowledged.

[1]A. A. Bokov and Z.-G. Ye, J. Mater. Sci. **41**, 31 (2006).
[2]R. Blinc, A. Gregorovič, B. Zalar, R. Pirc, V. V. Laguta, and M. D. Glinchuk, Phys. Rev. B **63**, 024104 (2000).
[3]G. Burns and F. H. Dacol, Phys. Rev. B **28**, 2527 (1983).
[4]J. Toulouse, F. Jiang, O. Svitelskiy, W. Chen, and Z. G. Ye, Phys. Rev. B **72**, 184106 (2005).
[5]E. Dul'kin, M. Roth, P.-E. Janolin, and B. Dkhil, Phys. Rev. B **73**, 012102 (2006).
[6]M. Roth, E. Mojaev, E. Dul'kin, P. Gemeiner, and B. Dkhil, Phys. Rev. Lett. **98**, 265701 (2007).
[7]B. Mihailova, B. Maier, C. Paulmann, T. Malcherek, J. Ihringer, M. Gospodinov, R. Stosch, B. Güttler, and U. Bismayer, Phys. Rev. B **77**, 174106 (2008).
[8]E. Dul'kin, B. Mihailova, M. Gospodinov, and M. Roth, Europhys. Lett. **94**, 57002 (2011).
[9]I. Gregora, *Raman Scattering* (Wiley, 2006), Chap. 2.3, pp. 314–328.
[10]B. Mihailova, R. Angel, B. J. Maier, A.-M. Welsch, J. Zhao, M. Gospodinov, and U. Bismayer, IEEE Trans. Ultrason. Ferroelectr. Freq. Control **58**, 1905 (2011).
[11]M. Wojdyr, J. Appl. Crystallogr. **43**, 1126 (2010).
[12]B. Mihailova, U. Bismayer, B. Güttler, M. Gospodinov, and L. Konstantinov, J. Phys.: Condens. Matter **14**, 1091 (2002).
[13]A.-M. Welsch, B. J. Maier, B. Mihailova, R. J. Angel, J. Zhao, C. Paulmann, J. M. Engel, M. Gospodinov, V. Marinova, and U. Bismayer, Z. Kristallogr. **226**, 126 (2011).
[14]U. Bismayer, V. Devarajant, and P. Groves, J. Phys.: Condens. Matter **1**, 6977 (1989).
[15]E. K. H. Salje and U. Bismayer, Phase Transitions **63**, 1 (1997).
[16]I. W. Chen, J. Phys. Chem. Solids **61**, 197 (2000).
[17]K. Z. Baba-Kishi and M. Pasciak, J. Appl. Crystallogr. **43**, 140 (2010).
[18]N. Waeselmann, B. Mihailova, B. J. Maier, C. Paulmann, M. Gospodinov, V. Marinova, and U. Bismayer, Phys. Rev. B **83**, 214104 (2011).
[19]D. La-Orauttapong, J. Toulouse, Z. G. Ye, W. Chen, R. Erwin, and J. L. Robertson, Phys. Rev. B **67**, 134110 (2003).
[20]P. Liu and X. Yao, Solid State Commun. **134**, 809 (2004).
[21]M. Wolters, C. L. H. Thieme, and A. J. Burggraaf, Mater. Res. Bull. **11**, 315 (1976).
[22]E. Dul'kin, B. Mihailova, G. Catalan, M. Gospodinov, and M. Roth, Phys. Rev. B **82**, 180101 (2010).
[23]V. Marinova, B. Mihailova, T. Malcherek, C. Paulmann, K. L. L. Kovacs, M. Veleva, M. Gospodinov, B. Güttler, and R. S. U. Bismayer, J. Phys.: Condens. Matter **18**, L385 (2006).
[24]A.-M. Welsch, B. Mihailova, M. Gospodinov, R. Stosch, B. Güttler, and U. Bismayer, J. Phys.: Condens. Matter **21**, 235901 (2009).
[25]E. Dul'kin, B. Mihailova, M. Gospodinov, and M. Roth, J. Appl. Phys. **112**, 064107 (2012).